Electric Power Systems Research 196 (2021) 107202

Contents lists available at ScienceDirect

Electric Power Systems Research

journal homepage: www.elsevier.com/locate/epsr

High impedance fault modeling and location for transmission line☆

Jose Doria-García [a,b,*], Cesar Orozco-Henao [a], Roberto Leborgne [b], Oscar Danilo Montoya [d,e], Walter Gil-González [c]

[a] Department of Electrical and Electronic Engineering, Universidad del Norte, Barranquilla, Colombia
[b] Electrical Engineering Postgraduate Program, Universidade Federal do Rio Grande do Sul, Porto Alegre, Brazil
[c] Facultad de Ingeniería, Institución Universitaria Pascual Bravo, Medellín, Colombia
[d] Facultad de Ingeniería, Universidad Distrital Francisco José de Caldas, Bogotá D.C., Colombia
[e] Smart Energy Laboratory, Universidad Tecnológica de Bolívar, Cartagena, Colombia

ARTICLE INFO

Keywords:
Distributed parameters
Electrical power systems
Fault location
High impedance fault
Nonlinear arcing fault

ABSTRACT

A fault in a power system generates economic losses, security problems, social problems and can even take human lives. Therefore, it is necessary to have an efficient fault location strategy to reduce the exposure time and recurrence of the fault. This paper presents an impedance-based method to estimate the fault location in transmission lines. The mathematical formulation considers the distributed parameters transmission line model for the estimation of the fault distance, and it is obtained by the application of Gauss-Newton method. Said method considers available voltage and current measurements at both terminals of the transmission line as well as the line parameters. Moreover, the method can be used for locating high and low impedance faults. Additionally, it is proposed an adjustable HIF model to validate its performance, which allows to generate synthetic high impedance faults by setting specific features of a HIF from simple input parameters. The error in fault location accuracy is under 0.1% for more than 90% of the performance test cases. The easy implementation of this method and encouraging test results indicate its potential for real-life applications.

Acronyms

DPFL:	Distributed Parameters Fault Location
EPS:	Electric Power Systems
FL:	Fault Location
HIF:	High Impedance Fault
LIF:	Low Impedance Fault

1. Introduction

An efficient protection scheme not only ensures that the system operates properly but also protects equipment, operating personnel and users [1]. Therefore, the electrical power quality, especially the continuity of service, is an issue that concerns both academics and entrepreneurs in the electricity sector. It is impossible to avoid some events that threaten the continuity of the electricity supply, especially where environmental (thunderstorms and salinity among others) and operating conditions can increase the probability of system faults [2]. Despite safety regulations and fault prevention techniques, faults occur spontaneously and randomly due to different natural events, such as high winds, fallen trees, physical contact with animals, fires, equipment failure and human errors, among others [3]. Faults compromise the continuity of the electric power service, mainly damaging the comfort of the users and generating economic losses. Therefore, it is necessary to reduce the restoration time of these faults, demonstrating the importance of accurate Fault Location (FL) methods [4].

High Impedance Fault (HIF) occurs when an electrical conductor makes contact with a low conductivity surface generating low fault currents [5]. The magnitude of fault currents can similar of the load current or other normal operation variations in power systems such as sudden load variations, connection and disconnection of capacitor banks and transformer taps changing; so its detection is a complex task [6]. Some works about of HIF models and FL methods are found in the technical literature. Sections 1.1 and 1.2 present a review of these

☆This work was supported in part by the *Joven Investigador* program of Minciencias – Colombia. Also, this study was financed in part by the Coordenação de Aperfeiçoamento de Pessoal de Nível Superior - Brasil (CAPES) - Finance Code 001. Paper submitted to the International Conference on Power Systems Transients (IPST2021) in Belo Horizonte, Brazil June 6–10, 2021.

* Corresponding author.
E-mail address: jdoriad@uninorte.edu.co (J. Doria-García).

https://doi.org/10.1016/j.epsr.2021.107202
Received 30 November 2020; Received in revised form 23 March 2021; Accepted 27 March 2021
Available online 7 April 2021

works.

1.1. HIF model review

The characteristics of HIF have been studied by some authors in [6,7]. The main features of HIF currents are listed below. *Non-linearity*: the relation between fault voltage and fault current is nonlinear. *Asymmetry*: The positive and negative half cycles have different peak values. The literature shows that usually the negative half cycle has greater magnitude. *Buildup*: The fault impedance varies over time from a large initial value to a lower final value. Therefore, the current transient starts at a small value increasing until reaching the maximum value. This period is known as *buildup*. *Shoulder*: time intervals or cycles where current magnitude remains constant during the *buildup* stage.

For a proper analysis of the effects of HIFs in power systems, an appropriate fault model must be implemented. One of the first publications on HIF was presented by [8] considering a resistance of great magnitude and constant value to emulate low magnitude currents. In [6] Emanuel's HIF model is represented as a series resistance and inductance to obtain low current magnitudes. In said model, two antiparallel DC sources and a pair of diodes are used to represent the asymmetric behavior of the Faults. Other antiparallel models are found in works such as [9]. Nam et al. [10] proposed a further model, in which the fault impedance is simulated through two variable resistors controlled by TACS in the ATP software. A resistor $R_1(t)$ is used to emulate the asymmetry and non-linearity in the steady state of the HIF, while $R_2(t)$ represents the transitory state where the buildup and shoulder stage are present.

Later, Santos proposed a variation to the Nam's model estimating $R_1(t)$ in a similar way [11]. However, from experimental measurements, Santos defined the resistance $R_2(t)$ as the polynomial (1). The polynomial coefficients take different values depending on the type of soil, such as sand, asphalt, and grass, among others. This model correctly represents the parameters of a HIF; nevertheless, the parameters used are unique and specific for the surface where the tests were carried out. Finally, Ferraz modified Emanuel's model by using a variable resistor which was determined similarly to the resistance $R_2(t)$ in the Santos model [12]. Ferraz model is not difficult to implement and successfully reproduces the four main characteristics of HIFs.

1.2. Fault location related works

The FL process is commonly studied for Low Impedance Faults (LIF) [13–15]. However, due to the non-linear nature of High Impedance Faults, specialized methods should be proposed [16,17]. To study the HIF location process, three general approaches are adopted: traveling waves, circuit analysis in time domain and circuit analysis in frequency domain. Each approach is briefly presented below.

The first approach is presented in [18] and [19], showing the principle of traveling waves with the wavelet transform. HIF generate a non-linearity in the EPS, particularity the one used by [20] to locate the fault point. These solutions are affected by extremely small current variations. Also, requiring a high amount of equipment increases the implementation cost of these techniques.

For the second approach, methods based on circuit analysis in the time domain were studied in [21,22]. In [21] a method based on a time domain formulation using least squares is proposed. It uses measurements of voltage and current at one-line-terminal but is strongly affected by its sensitivity to the HIF model. In [22], it is proposed a two-line-terminal formulation for locating fault by solving an optimization problem.

In [17,23,24], the circuit analysis in frequency domain is studied. Using this approach, a HIF location mathematical formulation was developed in [23]. In [24], a similar work was made, although based on apparent impedance. In addition to using frequency domain, the formulation was composed of a parameter estimation using the least square method. The first and third harmonic frequencies were considered in the development of the HIF location method. For this purpose, synchronized phasor measurement units (PMUs) are used in both terminals of a transmission line, allowing the estimation of the fault distance.

1.3. Contributions

The main contributions presented in this article are the following:

i A fault location method for transmission lines which does not depend on the HIF model, considering the distributed parameter model.
ii The proposed formulation can be applied to both high and low impedance fault location.
iii An adjustable HIF model that allows generating synthetic high impedance faults to reproduce specific behaviors in fault current features, such as number of shoulders and current magnitudes, among others.

The remaining of this paper is organized as follows. Section 2 describes the proposed adjustable HIF model. Section 4 presents the generalized mathematical formulation for the fault distance estimation. Section 4 presents a case study and results analysis. The conclusions are presented in Section 5.

2. High impedance fault model

This section presents an adjustable high impedance fault model. The proposed model, shown in Fig. 1, is a modification to the Ferraz model [12]. The HIF is modeled as a series of resistance with an inductance. Ferraz performed tests to record the current of a HIF and characterized the fault resistance on different contact surfaces: sand, soil, asphalt, grass, and tree. The polynomial given by (1) represents the fault resistance, $R_F(t)$ over time.

$$R_F(t) = \begin{cases} a_n t^n + a_{n-1} t^{n-1} + \ldots + a_1 t + a_0, & t < \Delta t \\ a_0, & t \geq \Delta t \end{cases} \quad (1)$$

In this research, an alternative function is proposed to adjust $R_F(t)$ with a smaller number of parameters. A statistical data analysis software, Statgraphics®, was used to obtain the regression that best fit the data and values of the fault resistance curve for each contact surface. It was determined that for most cases, the expression that best fit the data was the negative exponential defined by (2).

$$R_F(t) = C_1 e^{-C_2\sqrt{t}} \quad (2)$$

Subsequently, from the empirical analysis of the time-varying

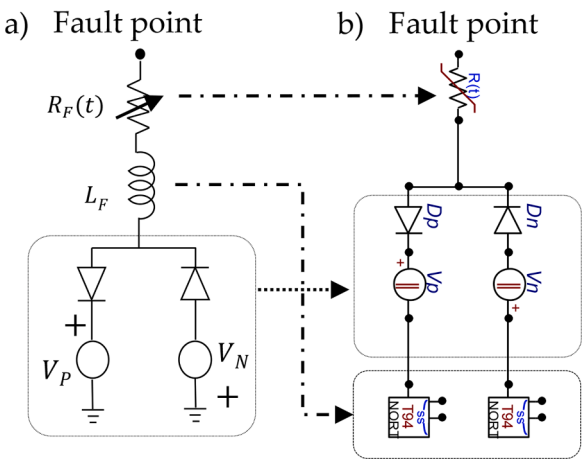

Fig. 1. a) Proposed HIF model. b) HIF model implementation in ATP.

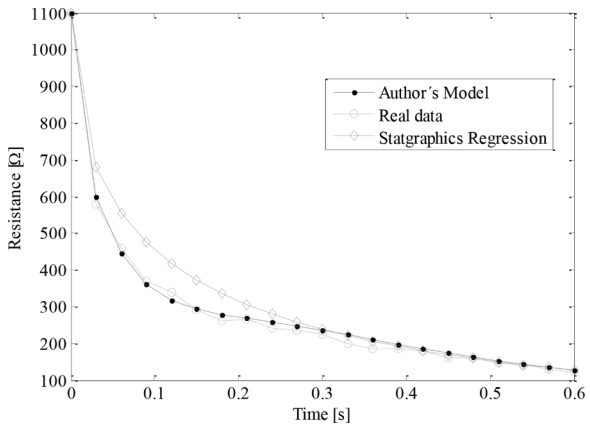

Fig. 2. Curve fitting comparison.

behavior of the fault resistance, an oscillation factor is added to the model according to (3). Fig. 2 compares the results of the curve fitting between the proposed HIF model (Author's Model), the initial one proposed by Statgraphics® and the original data for the HIF in sand surface.

$$R_F(t) = C_1 e^{-C_2\sqrt{t}} + C_3 e^{-C_4 t}\sin(C_5 t) \tag{3}$$

The model improves curve fitting and the coefficient of determination R^2 of the regression. Table A1 presents the model coefficients, $C_1,\ldots,C_5$, which best fit the Ferraz data for the cases: sand, soil, asphalt, grass, and tree. Fig. A1 shows the fault resistance results for the tests on the different surfaces.

2.1. Understanding the HIF model

The non-linearity and buildup and shoulder characteristics are introduced by the non-linear resistance $R_F(t)$ and the inductance. Each coefficient of the model, $C_1,\ldots,C_5$, is related to a particular feature of the HIF. The model allows simulating faults with specific features that we need to analyze. Defining the parameters R_0, R_f, N_s, α, A and t_{end} as:

- R_0: Initial resistance [Ω] value when starting fault.
- R_f: Final resistance [Ω] value once the steady state is reached.
- N_s: Number of shoulders presented by the HIF current.
- t_{end}: Fault duration [s] transient before clearing or self-extinction of the fault.
- A: Amplitude (percentage of R_0 [%]), related to HIF current peaks.
- α: attenuation coefficient, decay factor of current peaks. $\alpha \in (0,1]$. If $\alpha \approx 0$, A decays instantaneously to 0. For $\alpha = 1$, the amplitude drops to 5% at time t_{end}.

Therefore, the fault resistance model coefficients are set as shown from (4) to (8).

$$C_1 = R_0 \tag{4}$$

$$C_2 = \left(\frac{1}{\sqrt{t_{end}}}\right) Ln\left(\frac{R_0}{R_f}\right) \tag{5}$$

$$C_3 = A{\cdot}R_0 \tag{6}$$

$$C_4 = -\frac{Ln(0.05)}{\alpha t_{end}} \tag{7}$$

$$C_5 = N_s\left(\frac{2\pi}{t_{end}}\right) \tag{8}$$

In addition, two DC sources (V_P and V_N) and a pair of diodes (D_P and D_N) are used to represent the asymmetric behavior of the Faults. During the positive cycle of the voltage signal, once it exceeds the voltage value of V_P, D_p will allow current flow, while D_n does not allow current to pass through. In the negative cycle, the current flows through Diode N, once $V < V_N$, and not through Diode P. The HIF asymmetry is regulated by setting different values for V_P and V_N. To reproduce currents with greater magnitude in the negative cycle, the value of V_N must be greater than V_P, and vice versa.

Table 1
Input parameters and model coefficients, case study.

Input parameters	R_0	R_f	N_s	t_{end}	A	α
	700 Ω	100 Ω	5	0.63 s	20%	1/5
Model coefficients	C_1	C_2	C_3	C_4	C_5	t_{start}
	700	2.4516	140	23.7756	49.866	0.1

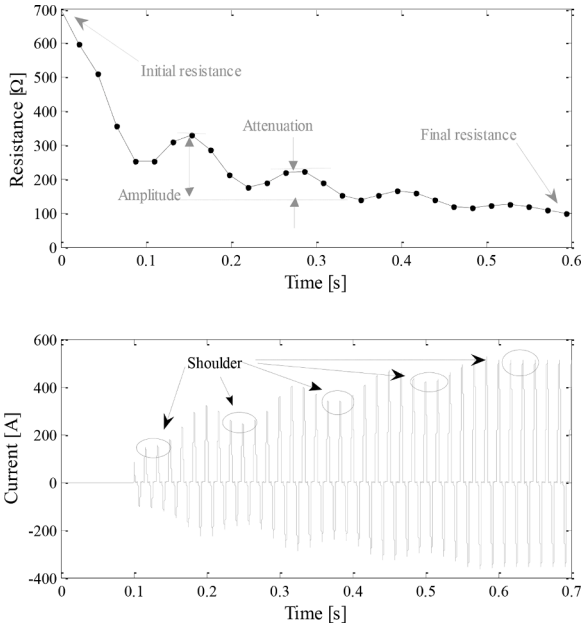

Fig. 3. Modeling case study. a) Fault resistance. b) HIF current.

2.2. HIF model: case study

This section seeks to show the application of the proposed model to generate a HIF with initial and final resistance of 700 Ω and 100 Ω, respectively. In addition, the fault current presents five shoulder events and current peaks due to an amplitude A of 20% of R_0. Factor A decays to 5% of R_0 in a fifth of the duration of the fault. The fault starts in 0.1 s and has a self-extinguishing time of 0.6 s. Table 1 summarizes the parameters and model coefficients for the case study.

Fig. 3a shows the fault resistance. The final and initial resistance conditions are met. On the other hand, Fig. 3b shows the fault current obtained from the model implementation. In Fig. 3b the 5 shoulder events can be observed.

The results are satisfactory since the proposed model manages to

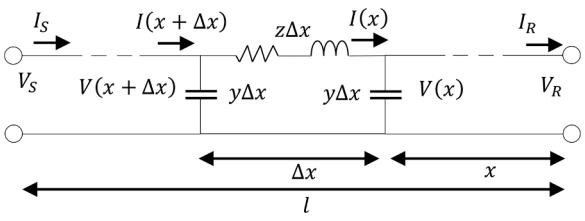

Fig. 4. Distributed Line Model.

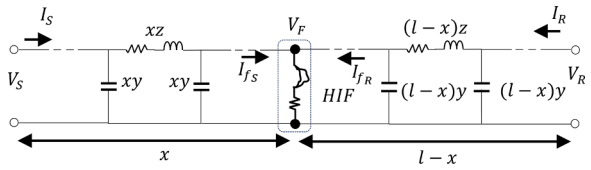

Fig. 5. Faulted distributed transmission line.

create a synthetic HIF with previously defined features. This will allow evaluations, tests, and simulations of a wide range of fault events for HIF fault location methods.

3. Fault location method

This section presents a FL method for a transmission line modelled by distributed parameter (DPFL). Fig. 4 shows an equivalent single phase transmission line model with distributed parameters, including series impedance, $z = r + j\omega L$, shunt admittance, $y = g + j\omega C$, and length l. In Fig. 5, V_S, V_R, I_S and I_R are the voltages and currents at the sending end and receiving end of the line, respectively [25].

Using Kirchhoff's Voltage and Current Laws and solving the differential equations [25], the well-known two port transmission line model is obtained (9):

$$\begin{bmatrix} V_R \\ I_R \end{bmatrix} = \begin{bmatrix} D & -B \\ -C & A \end{bmatrix} \begin{bmatrix} V_S \\ I_S \end{bmatrix} \tag{9}$$

Where,

$$A = D = \cosh\gamma l \tag{10}$$

$$B = Z_c \sinh\gamma l \tag{11}$$

$$C = \frac{B}{Z_c^2} = \frac{1}{Z_C}\sinh\gamma l \tag{12}$$

A good approximation to the hyperbolic function for lines up to 500 *km* is given by (13) to (15).

$$A = D \approx 1 + \frac{zy}{2}l^2 \tag{13}$$

$$B \approx zl\left(1 + \frac{zy}{6}l^2\right) \tag{14}$$

$$C \approx yl\left(1 + \frac{zy}{6}l^2\right) \tag{15}$$

Consider a HIF in the line of length l shown in Fig. 5. Where, V_S, V_R, I_S and I_R are the voltages and currents at sending and receiving buses, respectively; z is the series impedance per unit length; y is the shunt admittance; V_F is the voltage at fault point; I_{F_S} and I_{F_R} are the fault currents contribution from bus S and bus R, respectively; and x is the fault distance.

From Eq. (9),

$$V_F = D_x V_S - B_x I_S \tag{16}$$

$$V_F = D_{(l-x)} V_R - B_{(l-x)} I_R \tag{17}$$

Where, from (13) and (15),

$$D_x = 1 + \frac{zy}{2}x^2 \tag{18}$$

$$B_x = zx + \frac{z^2 y}{6}x^3 \tag{19}$$

$$D_{(l-x)} = 1 + \frac{zy}{2}(l-x)^2 \tag{20}$$

$$B_{(l-x)} = z(l-x) + \frac{z^2 y}{6}(l-x)^3 \tag{21}$$

Replacing (18) and (19) in (16) we have (22). Likewise, replacing (20) and (21) in (17) we have (23).

$$V_F = \left(1 + \frac{zy}{2}x^2\right)V_S - \left(zx + \frac{z^2 y}{6}x^3\right)I_S \tag{22}$$

$$V_F = \left(1 + \frac{zy}{2}\left(l^2 - 2lx + x^2\right)\right)V_R - \left(z(l-x) + \frac{z^2 y}{6}\left(l^3 - 3l^2 x + 3lx^2 - x^3\right)\right)I_R \tag{23}$$

Equating (22) to (23), we obtain (24).

$$b = a_1 x + a_2 x^2 + a_3 x^3 \tag{24}$$

Where,

$$b = V_S - V_R - \frac{zyl^2}{2}V_R + zlI_R + \frac{yz^2 l^3}{6}I_R \tag{25}$$

$$a_1 = z\left(I_S - ylV_R + I_R + \frac{yzl^2}{2}I_R\right) \tag{26}$$

$$a_2 = -\frac{yz}{2}(V_S - V_R + zlI_R) \tag{27}$$

$$a_3 = \frac{yz^2}{6}(I_S + I_R) \tag{28}$$

Eq. (24) is nonlinear due to the quadratic and cubic terms. A solution using *Non-Linear Least Squares* can be used to solve the problem of estimating the fault distance [26]. The *Gauss-Newton* method is proposed to determine the value of $\hat{x}$ that minimizes the estimation error in Eq. (29).

$$b = a_1\hat{x} + a_2\hat{x}^2 + a_3\hat{x}^3 + \xi \tag{29}$$

Where b, a_1, a_2 and a_3 are the set of voltage and current of N phasors according to (30). The set of N phasor are calculated from the fundamental component of the voltages and current [17].

$$b = \begin{bmatrix} b_{n_0} \\ \vdots \\ b_{n_0+(N-1)} \end{bmatrix} a_1 = \begin{bmatrix} a_{1n_0} \\ \vdots \\ a_{1n_0+(N-1)} \end{bmatrix} \\ a_2 = \begin{bmatrix} a_{2n_0} \\ \vdots \\ a_{2n_0+(N-1)} \end{bmatrix} a_3 = \begin{bmatrix} a_{3n_0} \\ \vdots \\ a_{3n_0+(N-1)} \end{bmatrix} \tag{30}$$

Consider $R(x)$ the residue vector and $J(x)$ the Jacobin matrix of $R(x)$, defined by (31) and (32), respectively.

$$R = \xi = a_1 x + a_2 x^2 + a_3 x^3 - b \tag{31}$$

$$J = \frac{dR}{dx} = a_1 + 2a_2 x + 3a_3 x^2 \tag{32}$$

In this way, the problem solution for x is given by the following iterative process (Algorithm 1), where s_{GN} is the step for the *Gauss-Newton* method.

3.1. Application of the proposed method for LIF

Since the DPFL method does not depend on the HIF model, the formulation can be applied for LIF. For a linear LIF fault, the set of voltage and current phasors used in (30) will be nearly the same. Thus, for a_1, a_2 and a_3, $[a_i]_{n_0} \approx [a_i]_{n_0+1} \approx \cdots \approx [a_i]_{n_0+(N-1)}$ and $[b]_{n_0} \approx [b]_{n_0+1} \approx \cdots \approx [b]_{n_0+(N-1)}$.

Consequently, when evaluating (31) and (32), $[R]_{n_0} \approx [R]_{n_0+1} \approx \cdots \approx [R]_{n_0+(N-1)} \approx R$ and $[J]_{n_0} \approx [J]_{n_0+1} \approx \cdots \approx [J]_{n_0+(N-1)} \approx J$. Applying the *Gauss-Newton* method in Algorithm 1, the step s_{GN} could be computed

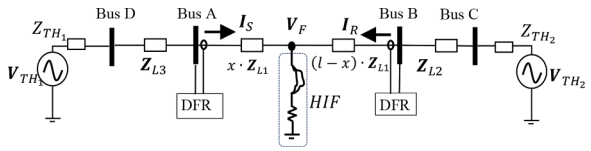

Fig. 6. Single-line diagram of the test EPS.

Table 2
Parameters of the test EPS.

External system		
Source S1		Source S2
$V_{TH1} = 229.174\angle 0°$ [kV]		$V_{TH2} = 228.353\angle 21.8°$ [kV]
$Z_{TH1} = 0.238 + j5.7132[\Omega]$		$Z_{TH2} = 0.238 + j6.19[\Omega]$
Line parameter		
$Z_L = 0.1137 + j0.7685[\Omega/km]$		$Y_L = j0.3295[\mu S/km]$
Length $L1$: 80 km	Length $L2$: 15 km	Length $L3$: 20 km

Table 3
Input parameters model, case study 1.

Contact Surface	R_0	R_f	N_s	A	α	t_{end}
Sand-1	1100	120	4	33%	0.29	0.63
Sand-2	700	120	4	33%	0.29	0.63
Sand-3	1100	120	7	33%	0.29	0.63
Sand-4	700	120	7	33%	0.29	0.63

Table 4
Input parameters model, case study 2.

Contact Surface	R_0	R_f	N_s	A	α	t_{end}
Surface 1	1360	140	5	15%	0.20	0.50
Surface 2	620	90	6	25%	0.16	0.45
Surface 3	1450	230	5	30%	0.22	0.60
Surface 4	400	80	7	15%	0.1	0.35

from (33) as shown in (34).

$$s_{GN} = \left(\sum_{i=1}^{N} J^2\right)^{-1}\left(\sum_{i=1}^{N} JR\right) = \frac{NJR}{NJ^2} = \frac{R}{J} \tag{34}$$

This proves that the DPFL method estimates the distance for both high and low impedance faults.

4. Case study description

The single-phase equivalent of the EPS of Fig. 6 is considered to evaluate the performance of the method in all case studies. The test system is connected between two external systems S1 and S2, represented by the external equivalent V_{TH} and $Z_{TH;}$ and includes a set of 3 lines L1-L3. The faults will be allocated in the main line L1. The system parameters are shown in Table 2. For the analysis, the faults are simulated in the range from 0% to 100% of the length of line.

The case studies carried out to evaluate the performance of the DPFL method are described below.

4.1. Performance of DPFL method vs initial resistance and N_S

In this case study, the performance of the method is analyzed against different HIF scenarios. Thus, tests were carried out considering HIF in sand surfaces, described in Table 3, to evaluate the response of the method to different values of initial fault resistance, R_0, and number of shoulders, N_S, in the HIF model. For this, the measured characteristic of the HIF in sand surface (Sand-1) was considered. Then, the initial fault resistance value was varied (Sand-2), as well as the number of shoulders (Sand-3) and both simultaneously (Sand-4).

4.2. DPFL performance vs variation of all HIF parameters

Additionally, the performance of the method for HIF events is analyzed once again by modifying all the parameters of the HIF model. Four test scenarios with synthetic fault resistance were carried out, changing the parameters R_0, R_f, N_S, A, α and t_{end}, as defined in Table 4.

4.3. DPFL performance vs transmission line length

The performance of the method was evaluated against different lengths of the line L1. Additional tests were carried out varying the length of the line L1 for values of 70, 80 and 90 km. The faults were simulated considering the Sand-1 contact surface described in Table 3.

4.4. DPFL performance vs fault initiation angle

Another case study was carried out to analyze the effect of the initiation angle in the proposed method. The effect of initiation angles of 0°, 30°, 60° and 90° were evaluated. The faults were simulated in the 80 km Line 1 and considering the Sand-1 surface.

4.5. DPFL performance for low impedance faults

As demonstrated in the mathematical formulation, the method does not depend on the fault model and, therefore, can be applied to LIF. A case study is carried out to evaluate the application of the DPFL method for LIF. In this scenario, simulations for LIF events are performed on the L1 line of the test EPS. The simulations considered a fault resistance of 10, 20, 30 and 40 Ω.

4.6. Sensitivity analysis

A sensitivity analysis was performed to determine the impact of noise and uncertainty on the accuracy of the method. For this, two scenarios were defined, as follows. Scenario 1: noise in the measurements. For this, the tests of the first scenario (L1 length 80 km and Sand-1) were repeated and a white Gaussian noise was added to the voltage and current measurements. A noise with a signal-to-noise ratio of 2% and 5% was added to the voltage and current measurements.

The scenario 2 shows the effect of uncertainties in the parameters of the line on the performance of the proposed method. The DPFL is based on impedance estimation, therefore, it is to be expected that errors in the line parameters will affect performance. The aim of this sensitivity analysis is to observe how the performance of the DPFL is affected by errors of up to 5% in the line parameters. For this, errors of ± 5% were added to the parameters of line L1.

4.7. Comparison test

Finally, the performance of the DPFL method was compared with the method proposed by the Ferraz [12,24], and with Doria's method [17]. The comparison is made for the case of L1 of 80 km and Sand-1 surface.

5. Results and discussion

This section presents the results for the performance evaluation and the sensitivity analysis for the test scenarios described in Section 4. The estimation error, ξ, is given by (35).

$$\xi = x_r - x_e \tag{35}$$

where, x_r is the real distance to fault point in km, and x_e is the distance estimated (km) by the proposed method.

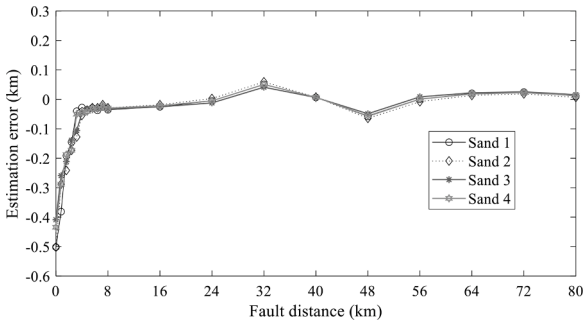

Fig. 7. Performance of DPFL method.

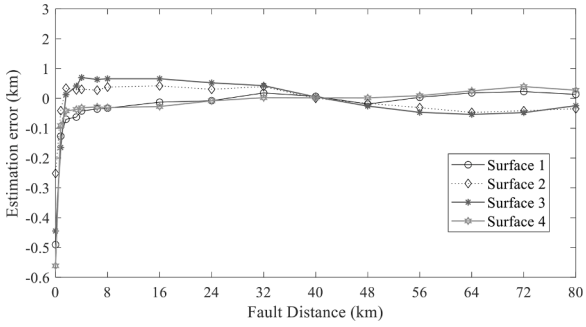

Fig. 8. DPFL performance vs variation of all HIF parameters.

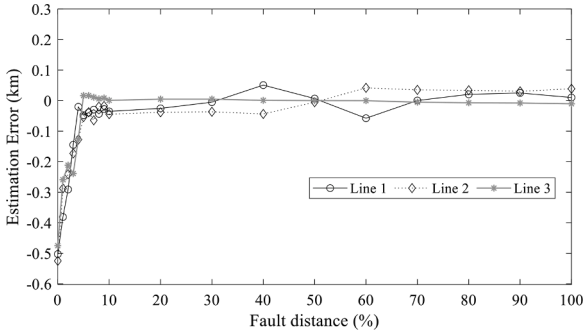

Fig. 9. DPFL performance vs line length.

5.1. Performance of DPFL method vs initial resistance and N_S

The performance and response of the proposed method is evaluated for different values of initial fault resistance, R_0, and number of shoulders, N_S. Fig. 7 shows the results obtained. The estimation error of the fault distance has a similar behavior for all fault events. For faults occurring at the beginning of the line, the error is less than 480 m for the line of 80 km, which corresponds to less than 0.6% of the total length. Negative estimation errors mean that the method is overestimating the true distance of the fault, that is, calculating a largest distance than the true one and vice versa. It is observed that the initial error decreases rapidly to less than 0.1% for faults estimates from 8 km to 80 km of the line. Also, it is observed that the results showed a strong convergence towards errors close to 0% as the fault location approaches close to 80 km. Moreover, no significant variance is observed in the response of the DPFL method for different values of R_0 and N_S.

5.2. DPFL performance vs variation of all HIF parameters

The results of the method validation for synthetic HIFs are shown in Fig. 8. The results show a behavior similar to those obtained in the previous scenario. The largest errors occur for faults at the beginning of the line, as well as convergence to errors close to 0 m when reaching 50% of the line. Furthermore, it can be appreciated that the DPFL method is not significantly sensitive to the HIF contact surface type. That is, the proposed FL method is independent and indifferent to the fault model. This shows great versatility in locating faults in a wide range of fault events.

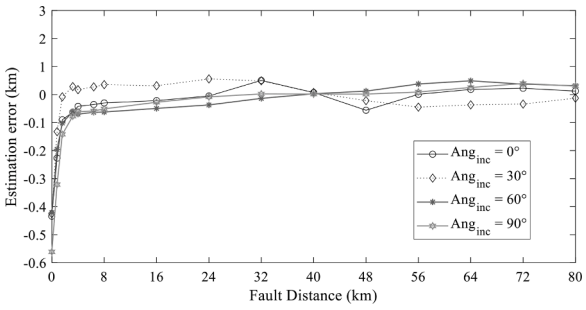

Fig. 10. DPFL performance vs initiation angle.

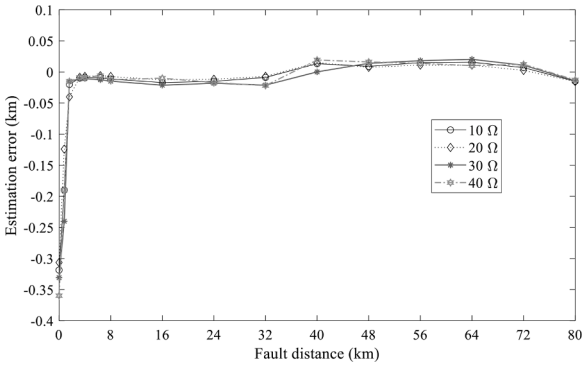

Fig. 11. Performance of method for LIF.

5.3. DPFL performance vs transmission line length

The results for the analysis of the performance of the DPFL for different line lengths are presented in Fig. 9. The characteristics observed in the previous case studies were again obtained. The error in estimation oscillates in the range of 100 m for almost 90% of the test for simulated faults, this is an error less than 0.1%. Likewise, for faults located at the beginning of the line, the largest errors occur, and the error is close to zero for faults at 50%.

5.4. DPFL performance vs fault initiation angle

The fault initiation angle was another factor analyzed in this work. The results in Fig. 10 indicate that there is no significant variation in the performance of the proposed method against this factor. The errors remain in the 0.1% range for almost 90% of the test scenarios.

5.5. DPFL performance for low impedance faults

The results obtained show that, indeed, the method can be applied to LIF, Fig. 11. The figure shows a behavior similar to the previous cases. The largest error is found at the beginning of the line, with a value lower than 360 m in all cases, which means less than 0.45%. Likewise, it is observed that the error decreases rapidly to the range of 50 m for faults between 8 km to 80 km, less than 0.06%.

Once again, as the fault locations approaches to 50% of the line, the error convergence towards 0%. Also, the fault resistance does not affect

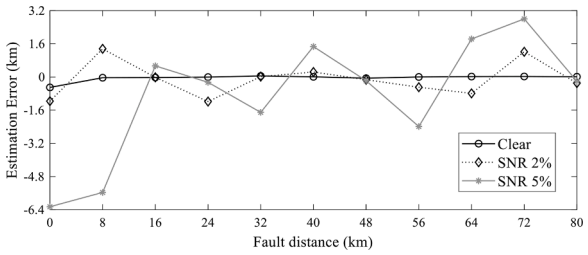

Fig. 12. Sensitivity analysis. a) SNR – 2%. b) SNR – 5%.

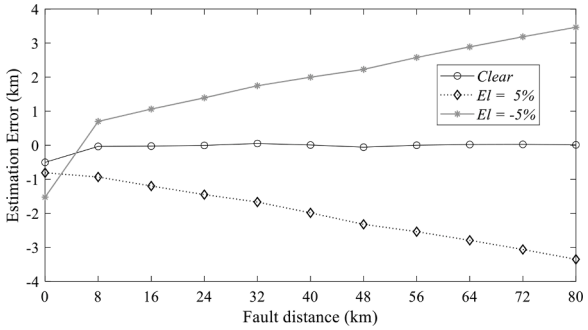

Fig. 13. Sensitivity analysis. Uncertainty of line parameter up to 5%.

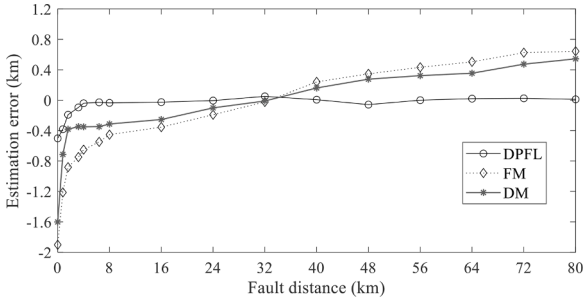

Fig. 14. Comparison test.

the distance estimation. The results of the test scenarios for the case studies are satisfactory.

5.6. Sensitivity analysis

The results of the sensitivity analysis are presented below. The first test scenario allows to analyze the effect of noise in the measurements on the performance of the DPFL, Fig. 12.

From Fig. 12 the error in the estimation increased due to the noise in the signal. For the case of 2% SNR, it is observed again that there is a tendency to errors close to 0% for faults nearly 50% of the line. While in the case of 5% SNR, this trend disappears, and the errors are more dispersed. The above shows the need to properly clean the signals previously to estimate the distance.

The second scenario of the sensitivity analysis allows evaluating the effect of uncertainties in the line parameters. The results in Fig. 13 show that the performance of the method is strongly affected by the uncertainties in the line parameters. In Fig. 13 for a 5% positive error in the line parameters, the estimation error is always negative. A positive error in the line parameters means that the real impedance of the line is lower, therefore, the method tends to estimate distances greater than the real ones, overestimation. In the opposite case, −5%, a tendency to underestimate the fault distance can be observed. The results show that the method is affected by uncertainties in the line parameters. Therefore, a correct parameterization of the line is highly recommended.

5.7. Comparison test

Fig. 14 shows the comparison test results. It is observed that the estimation error of the DPFL method remains in a range lower than 0.1 km, while the FM and DM methods present higher estimation errors. It is observed that both in FM and DM, there is a tendency to overestimate the distance for faults located in the first half of the line and underestimate for faults in the second half. The DPFL method presents a better performance in the evaluated scenario.

6. Conclusions

The proposed DPFL method considers the distributed parameter model of transmission lines including its capacitive effect. It was shown that the method is independent of the fault model can be applied to both HIF and LIF.

An extensive evaluation of test scenarios was carried out that allowed to validate the performance of the DPFL method. The error was less than 80 m for almost 90% of all faults of test performance scenarios, which corresponds to less than 0.1% of the line length. The highest error was less than 0.6% for faults at the beginning of the line, when the method tends to overestimate the distance.

Regarding the application of the method for LIF, the results were satisfactory with errors lower than 0.05% for almost 90% of the cases analyzed. Likewise, the comparative test showed a better performance for the proposed method.

Finally, an adjustable HIF model was presented. Results were satisfactory since it was possible to replicate the behavior of the HIF currents according to the parameters and characteristics presented in the literature. In addition, the model allows to set specific characteristics in the HIF current by modifying the characteristics of the non-linear resistance of the model from simple input parameters.

Authorship statement

All persons who meet authorship criteria are listed as authors, and all authors certify that they have participated sufficiently in work to take public responsibility for the content, including participation in the concept, design, analysis, writing, or revision of the manuscript. Furthermore, each author certifies that this material or similar material has not been and will not be submitted to or published in any other publication before its appearance in *Electric Power Systems Research - Journal*. We confirm that we have provided a current, correct email address which is accessible by the Corresponding Author and which has been configured to accept email from (jdoriad@uninorte.edu.co)

Author contributions

conceptualization, methodology, formal analysis, investigation, and writing-original draft preparation, Jose Doria-García, Cesar Orozco-Henao, Roberto Leborgne, Oscar Danilo Montoya, and Walter Gil-González.

Declaration of Competing Interest

The authors declare that they have no known competing financial interests or personal relationships that could have appeared to influence the work reported in this paper.

Appendix

Table A1 shows the coefficients that fit the different types of surface. Likewise, Fig. A1 shows the behaviors of resistance for each surface.

Table A1
HIF model coefficients.

Contact surface	C_1	C_2	C_3	C_4	C_5	R^2_{Stgrph}	R^2_{Author}
Sand	1100	2.79	−360	10	9.97	94.5%	98.9%
Ground	580	2.56	−98.6	5	19.94	92.1%	91.0%
Asphalt	1500	2.34	660	12	39.89	76.4%	87.5%
Grass	250	2.28	−170	14	19.94	85.9%	93.3%
Tree	550	2.31	−44	5	89.75	62.2%	91.7%

Algorithm 1

Set x_0

For $k = 0$ until converge

Compute $s_G N = -(J(x_k)^T J(x_k))^{(-1)} J(x_k)^T R(x_k)$. (33)

$x_{k+1} = x_k + s_{GN}$

Return

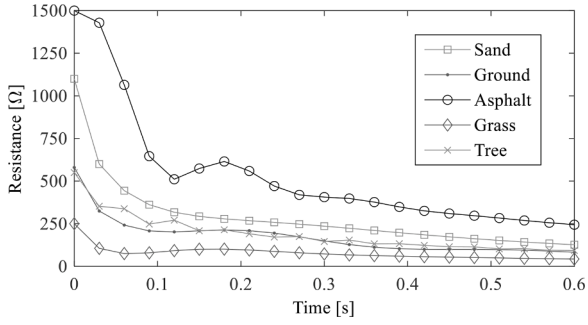

Fig. A1. Fault resistances test cases.

References

[1] PC37.250/D1.30, Nov 2019 - PC37.250/D1.30, Nov 2019 - IEEE Approved Draft Guide for Engineering, Implementation, and Management of System Integrity Protection Schemes - IEEE Standard n.d. https://ieeexplore.ieee.org/document/9031811 (accessed October 29, 2020).

[2] P Anderson, Analysis of Faulted Power Systems, Institute of Electrical and Electronics, Inc, Iowa, 1995.

[3] D. Hou, S. Carolina, D. Hou, S.E. Laboratories, Detection of high-impedance faults in power distribution systems, Power Syst. Conf. Adv. Metering, Prot. Control. Commun. Distrib. Resour. 2007 (2007) 1–11.

[4] M.M. Saha, J. Izykowski, E. Rosolowski, Fault Location on Power Networks, Springer, London, 2010.

[5] Ramamurthy T.A., Swarup K.S. High Impedance Fault detection using DWT for transmission and distribution networks. 2016 IEEE 6th Int Conf Power Syst 2016: 1–6. 10.1109/ICPES.2016.7584004.

[6] A.E. Emanuel, D. Cyganski, J.A. Orr, S. Shiller, E.M. Gulachenski, High impedance fault arcing on sandy soil in 15 kV distribution feeders: contributions to the evaluation of the low frequency spectrum, IEEE Trans Power Deliv 5 (1990) 676–686, https://doi.org/10.1109/61.53070.

[7] D.I. Jerrings, J.R. Linders, Ground resistance-revisited, IEEE Trans Power Deliv 4 (1989) 949–956, https://doi.org/10.1109/MPER.1989.4310592.

[8] M. Aucoin, Status of high impedance fault detection, IEEE Trans Power Appar Syst PAS-104 (1985) 637–644, https://doi.org/10.1109/TPAS.1985.318999.

[9] M. Jannati, L. Eslami, Precise modeling of high impedance faults in power distribution system in EMTPWorks software, J Electr Eng 13 (2013) 283–290.

[10] S.R. Nam, J.K. Park, Y.C. Kang, T.H. Kim, A modeling method of a high impedance fault in a distribution system using two series time-varying resistances in EMTP, Power Eng. Soc. Summer Meet. 2001. Conf. Proc. 2 (2001) 1175–1180, https://doi.org/10.1109/PESS.2001.970231.

[11] W. Santos, B. Sousa, N. Dantas, F. Bezzerra, M. Cerqueira, High impedance faults: from field tests to modeling, J Control Autom Electr Syst 24 (2013) 885–896.

[12] R.G. Ferraz, Localização De Faltas De Alta impedância: Formulação Baseada Na Impedância Aparente e Nométodo De Mínimos Quadrados, Universidade Federal do Rio Grande do Sul, 2014.

[13] R.A. de Aguiar, A.L. Dalcastagnê, H.H. Zürn, R. Seara, Impedance-based fault location methods: sensitivity analysis and performance improvement, Electr Power Syst Res 155 (2018) 236–245, https://doi.org/10.1016/j.epsr.2017.10.021.

[14] Akmaz D., Mamiş M.S., Arkan M., Tağluk M.E. Transmission line fault location using traveling wave frequencies and extreme learning machine. Electr. Power Syst. Res. 2018. 10.1016/j.epsr.2017.09.019.

[15] S.G. Di Santo, C.E.D.M. Pereira, Fault location method applied to transmission lines of general configuration, Int. J. Electr. Power Energy Syst. 69 (2015) 287–294, https://doi.org/10.1016/j.ijepes.2015.01.014.

[16] T. NengLing, C. JiaJia, Wavelet-based approach for high impedance fault detection of high voltage transmission line, Eur. Trans. Electr. Power 18 (2008) 79–92, https://doi.org/10.1002/etep.

[17] J. Doria-García, C. Orozco-Henao, L.U. Orozco Iurinic, J.D Pulgarín-rivera, High impedance fault location : generalized extension for ground faults, Electr. Power Energy Syst. 114 (2020), 105387, https://doi.org/10.1016/j.ijepes.2019.105387.

[18] H. Livani, C Yaman Evrenosoglu, A machine learning and Wavelet-Based fault location method for hybrid transmission lines, IEEE Trans. Smart Grid. 5 (2014) 51–59, https://doi.org/10.1109/TSG.2013.2260421.

[19] D.T.W. Chan, X. Yibin, A novel technique for high impedance fault identification, IEEE Trans. Power Deliv. 13 (1998) 738–744, https://doi.org/10.1109/61.686968.

[20] M. Chen, J. Zhai, Z. Lang, J. Liao, Z. Fan, High Impedance Fault Location in Transmission Line Using Nonlinear Frequency Analysis, Life Syst. Model Intell. Comput. 6328 (2010) 104–111.

[21] L.U. Iurinic, A.R. Herrera-Orozco, R.G. Ferraz, A.S. Bretas, Distribution systems high-impedance fault location: a parameter estimation approach, IEEE Trans. Power Deliv. 31 (2016) 1806–1814, https://doi.org/10.1109/TPWRD.2015.2507541.

[22] M. Ghazizadeh-Ahsaee, Accurate NHIF Locator Utilizing Two-End Unsynchronized Measurements 28 (2013) 419–426.

[23] C.J. Lee, J.B. Park, J.R. Shin, Z.M. Radojević, A new two-terminal numerical algorithm for fault location, distance protection, and arcing fault recognition, IEEE Trans. Power Syst. 21 (2006) 1460–1462, https://doi.org/10.1109/TPWRS.2006.876646.

[24] R.G. Ferraz, L.U. Iurinic, A.D. Filomena, D.S. Gazzana, A.S. Bretas, Arc fault location: a nonlinear time varying fault model and frequency domain parameter estimation approach, Int. J. Electr. Power Energy Syst. 80 (2016) 347–355, https://doi.org/10.1016/j.ijepes.2016.02.003.

[25] H. Saadat, Power System Analysis.Pdf, McGraw-Hill, New York, 1999.

[26] S. Gratton, A.S. Lawless, N.K. Nichols, Approximate Gauss-newton methods for nonlinear least squares problems, SIAM J Optim 18 (2007) 106–132, https://doi.org/10.1137/050624935.